DOI: 10.1002/ejic.200900773

Reduction vs. Metathesis in the Reactions of Bismuth Tribromide with a Bulky Lithium Silanide – An Experimental and Theoretical Study

Kirill Yu. Monakhov,[a] Thomas Zessin,[a] and Gerald Linti*[a]

Keywords: Bismuth / Silicon / Lithium / Crystal structure analysis / Density functional calculations

On reaction of $BiBr_3$ with $Li(thf)_3SiPh_2tBu$ (**1**) in the corresponding ratios redox/metathesis reactions were observed, yielding dibismuthane $(tBuPh_2Si)_4Bi_2$ (**2**) and disilylbismuth halide $(tBuPh_2Si)_2BiBr$ (**3**). The latter is a reaction intermediate in the formation of the dark-red **2**. The X-ray crystal structures of **1**–**3** were determined by low-temperature X-ray diffraction. The $Si_2Bi–BiSi_2$ core of **2** is in the semi-eclipsed conformation. No oligomerization of "nonthermochromic" **2** was observed. Compound **3** is a mixed substituted monomer with a pyramidal environment around the bismuth center. On the basis of quantum chemical calculations, the formation of tertiary bismuthane $(tBuPh_2Si)_3Bi$ is not expected for steric reasons. According to DFT-optimized geometries of the simplified model systems $n[(H_3Si)_2Bi]_2$ (n = 1–3), the closed-shell attraction between intermolecular Bi centers in the chain provides a moderate elongation of the intramolecular Bi–Bi bond in the dibismuthane unit and a shortening of the intermolecular Bi···Bi contacts. According to MP4(SDQ) computations, such oligomerization is carried out by intermolecular interaction of s lone pairs that are bound together and p-type orbitals of the Bi–Bi bonds in the bismuth chain. An increase in the number of $[(H_3Si)_2Bi]_2$ molecules *per* chain results in a decrease in the HOMO–LUMO gap and leads to a bathochromic shift. TD-PBE0 computations suggest that the lowest energy electron transition in **2** is metal–metal charge transfer. In addition, the attractive contributions in the chain $[(H_3A)_2Bi]_2\cdots[Bi(AH_3)_2]_2$ with silyl groups (A = Si) outweigh the repulsion of the Bi···Bi centers, whereas for the alkyl-substituted bismuth chain (A = C) the repulsive van der Waals force dominates. This fact makes the rectangle oligomerization model more preferred for $n[(H_3A)_2Bi]_2$ (A = C; n = 2), while for A = Si chain formation is favored in the gas phase.

Introduction

The chemistry of silyl-substituted bismuth compounds is an object of intensive study in the last years, because of the interesting behavior of these compounds in synthetic reactions and the following applications and the ability of these compounds to form interesting structural motives. Only seventeen examples of such species, whose structures have been determined by X-ray diffraction, are well-known up to now. Primarily, these are homonuclear[1–3] (four examples) and heteronuclear[1,3,5–11] complexes (thirteen examples) containing silyl groups of various steric requirements [$SiMe_3$, $SitBu_3$, $Si(SiMe_3)_3$], which play a stabilizing role here. In these compounds, bismuth displays the oxidation states +1, +2 and +3. Homo- and heteronuclear silyl-substituted bismuth complexes could be obtained by different synthetic strategies: (a) metalation of trisilylbismuthane with alkyllithium,[1] (b) conversion of lithium bis(trisilylbismuthane) with 1,2-dibromoethane,[1] (c) conversion of sodium potassium bismuthide with 1,2-dichlorotetramethyldisilane,[2] (d) reduction of bismuth halides with alkali metal silanides[3] and with silyl-substituted lithium phosphanides[4] {the formation of the silyl-substituted bismuth complexes from the reactions of $Ar'BiCl_2$ [Ar′ = 2,6-(2,6-iPr_2–C_6H_3)$_2$-C_6H_3] with potassium silanides was not observed},[12] (e) dehydrosilylation of group 13 diorganohydrides with trisilylbismuthane,[5,6,9] (f) heterometallic addition of trisilylbismuthane to group 13 trialkyl compounds,[6–8] (g) conversion of trisilylbismuthane with copper(I) *tert*-butoxide and trialkylphosphanes,[10] and (h) metathesis reaction of a heterometallic aluminum–bismuth adduct with a trialkyl indium–pyridine adduct.[11]

We report here on the redox and metathesis conversions of bismuth tribromide with the lithium silanide $Li(thf)_3SiPh_2tBu$[13] in various ratios, resulting in a stable silyl-substituted dibismuthane and a disilylbismuth halide. We also use quantum chemical calculations on simplified model compounds of silyl- and alkyl-substituted bismuthanes to obtain an insight into the possibility of forming $(R_3Si)_3Bi$ structures, the stability of the silyl-substituted $(H_3Si)_2E^{\cdot}$ radicals against dimerization as well as the instability of $[(H_3Si)_2E]_2$ molecules towards dissociation in the series of pnicogens E = P, As, Sb, Bi. In addition, the oligomerization of $n(H_3A)_2Bi^{\cdot}$ radicals (A = C, Si; n = 2–4), the bonding and orbital situations as well as the electronic excitations in the dibismuthane and its oligomerized forms were studied with use of density functional (DFT), time-dependent density functional (TD-DFT), and conventional ab ini-

[a] Anorganisch-Chemisches Institut, Universität Heidelberg, Im Neuenheimer Feld 270, 69120 Heidelberg, Germany
Fax: +49-6221-546617
E-mail: gerald.linti@aci.uni-heidelberg.de

tio theory to obtain an insight into the nature of Bi–Bi and Bi···Bi interactions, which could be observed in the fluid and crystalline phase.

Results and Discussion

Synthesis

The reactions of $BiBr_3$ with $Li(thf)_3SiPh_2tBu$ (**1**) in the corresponding ratios in the solvent toluene yield the silyl-substituted bismuthanes **2** and **3** (Scheme 1). Thus, the intended salt metathesis reaction of $BiBr_3$ with three equivalents of **1** leads to a redox process under the applied conditions (warming from –78 °C to room temp. during the reaction), resulting in the dibismuthane $(tBuPh_2Si)_4Bi_2$ (**2**) and the disilane $(tBuPh_2Si)_2$. During the reaction the color of the solution changes from green to red-brown. Workup allows isolation of **2** as dark-red crystals soluble in toluene. The ^{29}Si NMR spectrum of the dark-red solution contains two signals: singlets for the silicon atoms of dibismuthane (δ = 15.9 ppm) and disilane (δ = –2.16 ppm).

The formation of $(tBuPh_2Si)_3Bi$ was not observed. This is probably due to steric reasons, which will be discussed later.

Heating of **2** under reflux at 100 °C for 3 h did not lead to disproportionation into elemental bismuth and $(tBuPh_2Si)_3Bi$ or to dissociation of **2** into corresponding radicals. As a result, **2** could be observed in the reaction solution again as a thermodynamically stable compound. This high thermostability may be related to the relatively short Bi–Bi distance in **2**.

The reaction of $BiBr_3$ with **1** in a 1:2 and 1:1 ratio gives the disilylbismuth halide $(tBuPh_2Si)_2BiBr$ (**3**) together with **2**. Here, after workup of the reaction mixture, red crystals of **3** could be isolated from the dark-green hexane solution as well as from the red toluene solution only. The ^{29}Si NMR spectra of the solutions show singlets at δ = –4.19 and –6.10 ppm, respectively. In addition, both solutions contain **2**, which forms here predominantly (ratio ca. 2.5:1 according to ^{29}Si NMR signals). Interestingly, the dark-green solution is more stable than that of red color, which decomposes with formation of elemental bismuth after short periods of time at low temperature (–20 °C) or much faster at room temperature. In our opinion, the dark-green oily solution should contain a form of **3** oligomerized via weak Br–Bi···Br intermolecular contacts (like Mes_2BiBr,[14] for example), which are broken on dissolution of the oligomer to give **3**. However, no crystals could be isolated from this solution.

X-ray Crystal Structures

Single crystals of **1**–**3** suitable for X-ray structure determination were isolated from the corresponding solutions at –20 °C.

Tris(tetrahydrofuran)lithium(*tert*-butyldiphenylsilanide)-lithium [$Li(thf)_3SiPh_2tBu$ (**1**)] was synthesized by starting from the reaction of chloro-*tert*-butyldiphenylsilane, $tBuPh_2SiCl$, with lithium granulate in tetrahydrofuran solution according to the literature procedure.[13] The compound was crystallized from a *n*-hexane/thf mixture at –20 °C. Compound **1** crystallizes in the monoclinic crystal system, space group $P2_1/n$ (Table 3). Figure 1 shows the molecular structure of **1** in the solid state. The asymmetric unit contains three independent molecules of **1**. The crystal structure displays monomer silanide units, where the lithium ions are surrounded by three thf molecules and a silicon atom in a tetrahedral geometry. They differ only in the slight disorder of coordinated thf molecules and in the rotational conformation of the $(thf)_3Li$ and the $SiPh_2tBu$ units. For the $C_{Bu}SiLiO$, torsional angle values of 37°, 39°, and 49° are observed. The Si–Li bond lengths in the three independent molecules [266.0(5), 267.5(5), 269.0(5) pm] are fairly similar. This is in the typical range, as compared to other thf adducts of monomeric lithium silanides {262.7 pm in $Li(thf)_3SiPh(NEt_2)_2$,[15] 266.9 pm in $Li(thf)_3Si$-

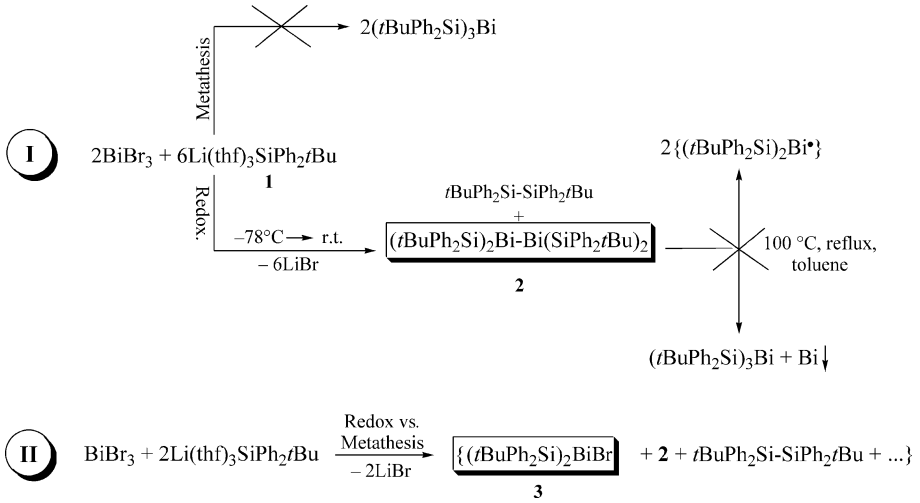

Scheme 1. Reaction pathways I and II leading to the formation of bismuthanes **2** and **3**.

$(SiMe_3)_3$,[16] 267.2 pm in $Li(thf)_3SiPh_3$,[16] 267.8 and 268.2 pm in $Li(thf)_3SiPh_2(NEt_2)$,[15] 271.7 pm in $Li(thf)_3Si\mathit{t}Bu_3$,[17,18] 273.2 pm in $Li(thf)_3SiPh_2(NPh_2)$,[19] and 276.0 pm in $Li(thf)_3Si(SiMe_2SiMe_3)_3$[20]}.

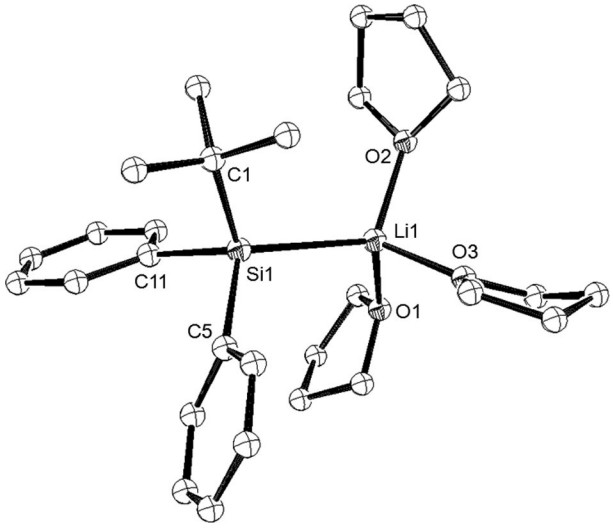

Figure 1. Molecular structure of lithium silanide **1** (crystal; the thermal ellipsoids are given at the 30% probability level; hydrogen atoms are omitted for clarity). Only one of the three independent molecules is shown. Selected bond lengths [pm] and angles [°]: Si1–Li1 267.5(5), Si1–C5 192.0(4), Si1–C11 192.7(4), Si1–C1 195.8(5), O1–Li1 198.1(8), O2–Li1 196.1(8), O3–Li1 192.4(8), C5–Si1–C11 99.8(2), C5–Si1–C1 106.3(2), C11–Si1–C1 102.2(2), O3–Li1–O2 105.1(3), O3–Li1–O1 99.1(4), O2–Li1–O1 106.8(3).

Compound **2** crystallizes in the triclinic crystal system, space group $P\bar{1}$, $Z = 2$ (Table 3, Figure 2). The solid-state molecular structure shows a dibismuthane with a Bi–Bi bond length of 300.6 pm. The $Si_2Bi–BiSi_2$ core is in the semi-eclipsed conformation, where each bismuth atom is surrounded by two *tert*-butyldiphenylsilyl ($\mathit{t}BuPh_2Si$) groups. Two silyl-containing dibismuthanes of similar structural type, but with less bulky silyl (Me_3Si) or alkyl [$(Me_3Si)_2CH$] groups, have been reported up to now.[1,21] The Bi–Bi distance in **2** is shorter by 2.9 pm and 4.7 pm than in antiperiplanar molecules $(Me_3Si)_4Bi_2$ ($d_{Bi–Bi}$ = 303.5 pm)[1] and $[(Me_3Si)_2CH]_4Bi_2$ ($d_{Bi–Bi}$ = 305.3 pm),[21] respectively. Finally, it is 3.4 pm shorter than the sum of the covalent radii ($\Delta\Sigma r_{cov}$ = 304 pm). The Bi–Si bond lengths in **2** are $d_{Bi–Si}$ = 268.6–270.8 pm, which is expected from the covalent radii of bismuth and silicon [$r_{cov}(Si) = 0.5r_{(Si–Si)}$, $r_{(Si–Si)}$ = 238.6 pm in $(\mathit{t}BuPh_2Si)_2$]. The molecules of **2** can be regarded as isolated ones with a shortest intermolecular Bi···Bi distance of 1000 pm. In $(Me_3Si)_4Bi_2$, aggregation via Bi···Bi contacts (380.4 pm) was observed.[1,22] This leads to a moderate elongation of the Bi–Bi bond in the dibismuthane unit. The quantum chemical calculations, which will be discussed later, provide evidence for this.

The space-filling representations of the silyl-substituted molecules **2** and $[(Me_3Si)_2Bi]_2$ in Figure 3 show that bulky $\mathit{t}BuPh_2Si$ groups of **2** more effectively surround the reactive

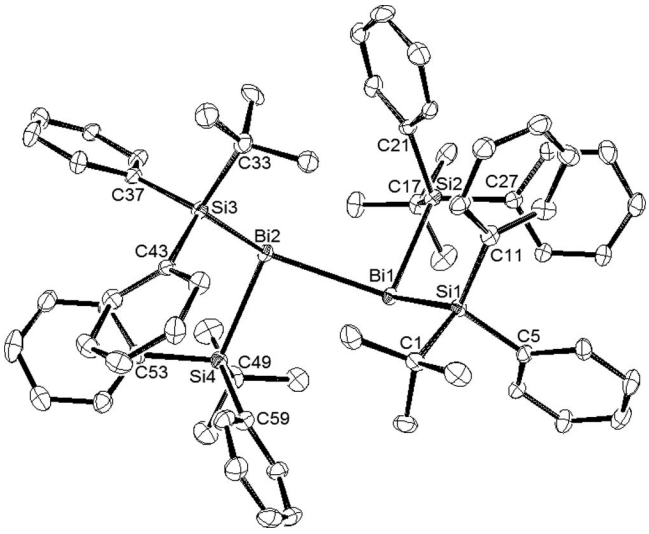

Figure 2. Molecular structure of **2** (crystal; the thermal ellipsoids are given at the 30% probability level; hydrogen atoms are omitted for clarity). Selected bond lengths [pm] and angles [°]: Bi1–Bi2 300.6(8), Bi1–Si2 268.9(2), Bi1–Si1 270.8(2), Bi2–Si4 268.6(3), Bi2–Si3 268.7(3), Si1–C11 187.8(9), Si1–C1 190.2(9), Si1–C5 191.4(9), Si2–C21 186.4(8), Si2–C27 187.1(9), Si2–C17 190.7(8), Si3–C43 187.5(8), Si3–C37 189.6(8), Si3–C33 191.3(10), Si4–C53 187.5(9), Si4–C59 188.3(8), Si4–C49 192.3(9), Si2–Bi1–Si1 101.63(7), Si2–Bi1–Bi2 93.87(6), Si1–Bi1–Bi2 124.58(6), Si4–Bi2–Si3 101.77(8), Si4–Bi2–Bi1 94.98(6), Si3–Bi2–Bi1 124.28(5), C11–Si1–C1 113.6(4), C11–Si1–C5 108.4(4), C1–Si1–C5 106.3(4), C11–Si1–Bi1 118.4(2), C1–Si1–Bi1 107.5(3), C5–Si1–Bi1 101.3(3), C21–Si2–C27 106.5(4), C21–Si2–C17 113.3(4), C27–Si2–C17 106.6(4), C21–Si2–Bi1 115.7(3), C27–Si2–Bi1 107.4(2), C17–Si2–Bi1 106.9(3), C43–Si3–C37 106.9(4), C43–Si3–C33 113.2(4), C37–Si3–C33 106.5(4), C43–Si3–Bi2 117.7(3), C37–Si3–Bi2 102.6(3), C33–Si3–Bi2 108.8(3), C53–Si4–C59 106.9(4), C53–Si4–C49 106.7(4), C59–Si4–C49 113.4(4), C53–Si4–Bi2 107.9(3), C59–Si4–Bi2 115.0(3), C49–Si4–Bi2 106.6(3), Si1–Bi1–Bi2–Si3 4.62(9), Si2–Bi1–Bi2–Si3 –102.36(8), Si1–Bi1–Bi2–Si4 –103.26(8), Si2–Bi1–Bi2–Si4 149.76(8).

Bi–Bi bond. Such effective steric protection of the bismuth centers in **2** can be regarded as one of the main reasons of the stability of this compound.

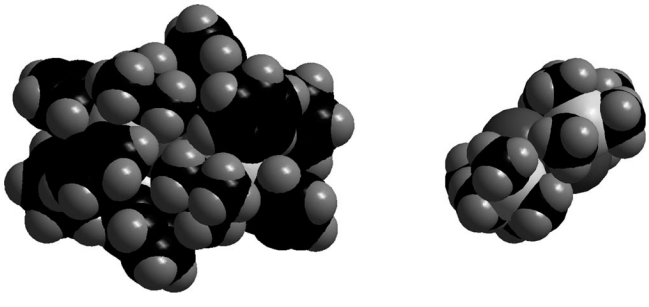

Figure 3. Space-filling models of silyl-substituted dibismuthanes **2** (left) and $[(Me_3Si)_2Bi]_2$ (right).

The bond angles around bismuth lie in the wide range of 94–125°, resulting in a sum of angles at the bismuth centers (Bi^{sum}) of 320.1° (Bi_1) and 321.0° (Bi_2). The dihedral angle τ between Si–Bi–Si planes is 84.1° (Figure 4). Thus, all of these angles are evidence of steric strain in **2**.

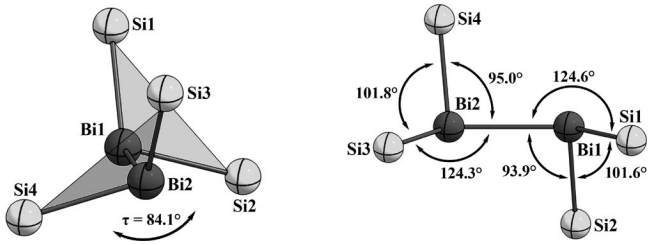

Figure 4. The core of dibismuthane **2**. Views along the Bi–Bi bond.

Compound **3** crystallizes in the orthorhombic crystal system, space group $P2_12_12_1$. Its solid-state structure (Table 3, Figure 5) is similar to $[(Me_3Si)_2CH]_2BiCl$,[23] which is described as a mixed-substituted monomeric diorganobismuth halide with a pyramidal environment around the bismuth center. The Bi–Si bond lengths in **3** are 267.8 pm and 269.6 pm, which are similar to the Bi–Si distances in **2**. The Bi–Br distance is 266.7 pm. The Si–Bi–Si angle is 100.22°. As in $[(Me_3Si)_2CH]_2BiCl$, we observed a slight dissimilarity of the R–Bi–X angles (Si–Bi–Br = 96.97° and 98.70°). Such slight distortions in the Bi–Si bond lengths and Si–Bi–Br angles may be related to steric strain in **3**. In addition, the total sum of angles at the bismuth center (Bi^{sum}) is 295.9°. This is a smaller deviation than that in **2** from the expected structure of R_3Bi with bond angles of 90° each.

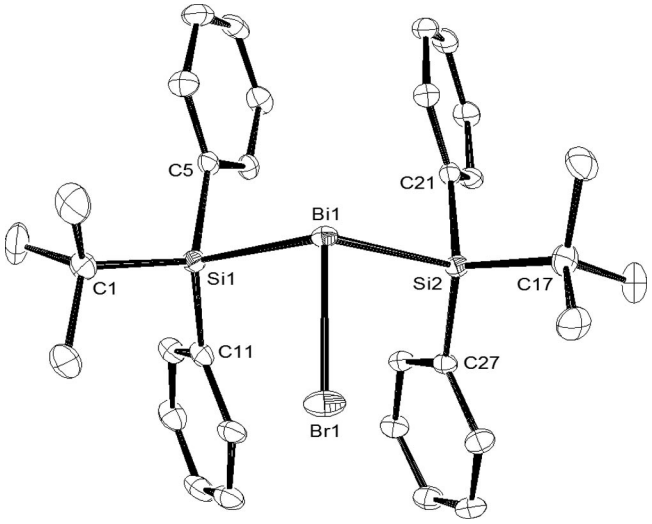

Figure 5. Molecular structure of **3** (crystal; the thermal ellipsoids are given at the 30% probability level; hydrogen atoms are omitted for clarity). Selected bond lengths [pm] and angles [°]: Br1–Bi1 266.7(7), Bi1–Si1 267.8(1), Bi1–Si2 269.6(1), Si1–C11 186.8(5), Si1–C5 187.4(4), Si1–C1 191.0(5), Si2–C27 186.3(4), Si2–C21 186.9(4), Si2–C17 189.8(5), Br1–Bi1–Si1 98.70(3), Br1–Bi1–Si2 96.97(3), Si1–Bi1–Si2 100.22(3), C11–Si1–C5 111.69(2), C11–Si1–C1 107.7(2), C5–Si1–C1 112.9(2), C11–Si1–Bi1 117.2(1), C5–Si1–Bi1 98.4(1), C1–Si1–Bi1 108.8(2), C27–Si2–C21 110.8(2), C27–Si2–C17 113.2(2), C21–Si2–C17 108.0(2), C27–Si2–Bi1 114.4(1), C21–Si2–Bi1 103.1(1), C17–Si2–Bi1 106.7(2).

As can be seen from the space-filling model of **3** (Figure 6), there is a vacant site on the bismuth atom, which is assigned to the lone pair (LP) on the bismuth atom. Through this LP, intermolecular interactions like Br–Bi···Br in the oligomerized form are enabled.

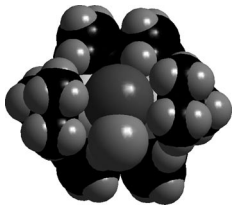

Figure 6. Space-filling models of disilylbismuth bromide **3**.

Quantum Chemical Calculations

Pyramidal $(R_3Si)_3Bi$ Structures

The possibility of forming $(R_3Si)_3Bi$ structures may be related to a "hybridization sp valence orbitals effect" of the metal, to the presence of the lone pair on the metal atom and its type, an orientation of the lone pair, and as a consequence the repulsive interactions of the R_3Si groups around metal center. Thus, according to the natural localized molecular orbitals (NLMO) analysis at the MP2(full) level on the DFT-optimized geometry of the simplified electrostatic model $(H_3Si)_3Bi$, the bismuth atom uses 9.3% s and 90.4% p orbitals for bonding with silyl groups [$s^{8.3\%}p^{91.4\%}$ according to the natural bond orbital (NBO)]. The lone pair of electrons on Bi possesses 74.6% s and 25.4% p character (according to the NLMO). As a result, the $(H_3Si)_3Bi$ structure shows a pyramidal environment around Bi (Figure 7), where the Si–Bi–Si angles are 89°. In NBO evaluations, the Bi–Si bonds are more weakly polarized toward Si atoms (ca. 50.7%). In this manner, the valence sp hybrid orbitals at Bi are adapted for a nucleophilic attack of only moderately bulky alkyl or silyl anions like $[(Me_3Si_2)AH]^-$ (A = C) or $[AMe_3]^-$ (A = Si) to form $(R_3A)_3Bi$.[24] Increased steric bulk of substituents leads to an increase in the Bi–Si bond lengths [267.0 pm for $(H_3Si)_3Bi$; 267.8 pm for $(Me_3Si)_3Bi$; 273.2–275.9 pm for $(iPr_3Si)_3Bi$] and the Si–Bi–Si angles [89.0° for $(H_3Si)_3Bi$, 96.8° for $(Me_3Si)_3Bi$, 107.1–109.7° for $(iPr_3Si)_3Bi$], and, consequently, to more steric strain in the molecule. Here, $(tBuPh_2Si)_3Bi$ is a good example. Thus, according to the DFT-optimized geometry of the tertiary bismuthane $(tBuPh_2Si)_3Bi$, the Bi–Si bond lengths and the Si–Bi–Si angles lie between 273.3 and 275.1 pm, and 99.6 and 109.8°, respectively. Such relatively large deviations in the Bi–Si distances and the Si–Bi–Si angles may be related to repulsive interactions of the silyl substituents in $(tBuPh_2Si)_3Bi$. Therefore, three bulky $tBuPh_2Si$ ligands may be hardly coordinated to the bismuth centre on the way of experimentally described reactions here, whereas for indium (for example), displaying a planar structural motive in the solid state, this is accessible {see $[(tBuPh_2Si)_3In]$}.[25]

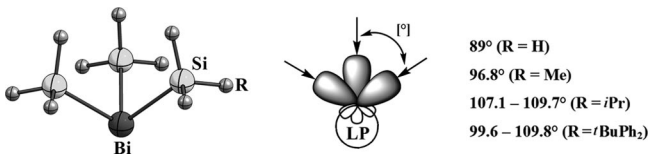

Figure 7. DFT-optimized structure for $(R_3Si)_3Bi$ (R = H, Me, *i*Pr, $tBuPh_2$) molecules and view of sp valence orbitals of metal.

Pnicogen Radicals $(H_3Si)_2E^{\cdot}$ and Their Dimers

Formation of persistent radicals $(R')_2E^{\cdot}$ (R′ = alkyl or amide) of group 15 elements is well known. Thus, the phosphanyl and arsinyl radicals,[26,27] generated in solution by reaction of the dialkyl- or diamidophosphorus(III) or -arsenic(III) monochlorides with an electron-rich olefin, or under photolytic conditions by melting or vaporizing of the dipnicogens [here, $(PR'_2)_2$], could be observed in solution as well as in the gas phase and characterized by ESR spectroscopy, gas-phase electron diffraction (GED), and X-ray crystal analysis. In addition, the participation of the group 15 p elements in the formation of the silyl radicals is established. For example, homolysis of tris(triethylsilyl)antimony led to antimony and free triethylsilyl radicals.[28] In case of bismuth, the formation of its $(R')_2Bi^{\cdot}$ radicals was observed in the gas phase. Thus, the signals for $(R')_2Bi^+$ ions [R′ = $(Me_3Si_2)CH$ or 2,6-$(Me_2NCH_2)_2C_6H_3$] could be detected by EI mass spectrometry.[21,29] The probable formation of the bismuth radicals in liquid ammonia was reported by Gilman.[30] Di-*p*-tolylbismuth halide and sodium reacted to yield an intensely green colored solution. The homolytic cleavage of the Bi–Bi single bond should depend on the steric bulk of the ligands. In our case, we could observe a bismuth cation $[(t\text{BuPh}_2\text{Si})_2\text{Bi}]^+$ in toluene solution by LIFDI mass spectrometry, indicating homolytic dissociation of the dibismuthane and subsequent ionization.

Herein, we discuss the stability of the silyl-substituted $(H_3Si)_2E^{\cdot}$ radicals towards dimerization, and thus, the instability of $[(H_3Si)_2E]_2$ molecules towards dissociation in the series of pnicogens E = P, As, Sb, Bi on the basis of the bond association and dissociation energies, respectively, as well as on the basis of the total charge transfer on the pnicogen atoms during both of these processes.

Upon traveling downward within group E, the bond length E–E in the $[(H_3Si)_2E]_2$ compounds becomes longer and the natural population analysis (NPA) pnicogen charge becomes more positive (Table 1, Figure 8). This is in line with the increasing covalent radii and decreasing electronegativity of the homologous elements. The relatively small increase in the Bi–Bi bond length compared to that in the Sb–Sb bond length may be related to "relativistic effects", which result in a decrease in the atom sizes and a shortening of the E–E bond. Upon dimerization of the pnicogen radicals, the association energies for $[(H_3Si)_2E]_2$ decrease within the group (Table 1, Figure 9). In addition, the total intramolecular charge transfer for the lighter elements becomes more negative; this corresponds to a better stabilization of the molecules by the formation of E–E bonds. As a consequence, the instability of the E–E bond increases within the group, which is expressed in a decrease in the bond dissociation energies of $[(H_3Si)_2E]_2$ molecules. Here, as expected, the longer the bond length, the less is the bond energy. The total charge transfer also indicates that the Bi–Bi bond is the most flexible among the E–E bonds of other pnicogens. The E–E bond strengths for $[(H_3Si)_2E]_2$ molecules (P–P > As–As > Sb–Sb > Bi–Bi), on the basis of the Wiberg bond indexes (WBIs) and the effective overlapping of orbitals,

Table 1. Intramolecular properties. Computed structural and bond strength parameters, and calculated charges and energies for molecules $[(H_3Si)_2E]_2$ (E = P, As, Sb, Bi) of C_{2h} symmetry.

Parameter	$(H_3Si)_2E–E(SiH_3)_2$ E = P	E = As	E = Sb	E = Bi
d(E–E)[a]	225.7	247.6	285.6	301.4
Q_{NPA}[b]	–0.3990	–0.2568	+0.0002	+0.0741
ΔQ_{ct}(as)[c]	–0.350	–0.320	–0.283	–0.234
ΔQ_{ct}(dis)[c]	+0.350	+0.320	+0.283	+0.234
WBI[c]	0.995	0.980	0.974	0.970
OOv[d]	0.761	0.722	0.719	0.658
ΔE_{as}[e]	–215.4	–188.8	–155.8	–141.3
ΔE_{dis}[e]	215.4	188.8	155.8	141.3

[a] E–E bond lengths [pm] were computed at the PBE0/BS-I level of theory. [b] The NPA pnicogen charges *e* were computed at the MP2(full)/BS-II//PBE0/BS-I level. [c] Total charge transfers (ΔQ_{ct}) *e* upon association (as) and dissociation (dis) and the Wiberg bond index (WBI) for E–E were calculated at the MP2(full)/BS-II//PBE0/BS-I level. [d] Order of overlapping (OOv) of the valence sp orbitals of the pnicogens was computed at the MP2(full)/BS-II//PBE0/BS-I level. [e] E–E bond association (ΔE_{as}) and bond dissociation (ΔE_{dis}) energies [kJ/mol] were calculated at the MP4(SDQ)/BS-II//PBE0/BS-I level.

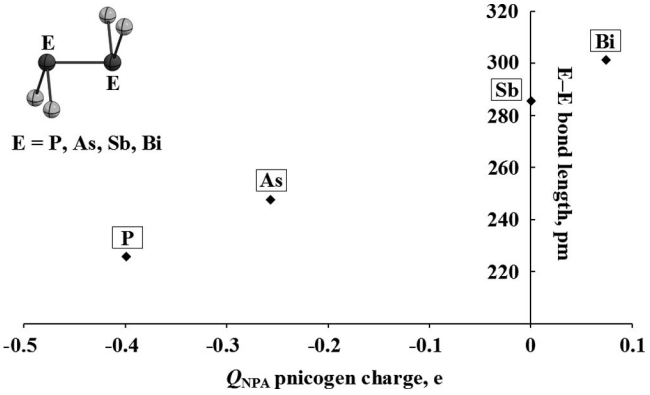

Figure 8. Calculated bond lengths and NPA pnicogen charges for $[(H_3Si)_2E]_2$ (A = P, As, Sb, Bi).

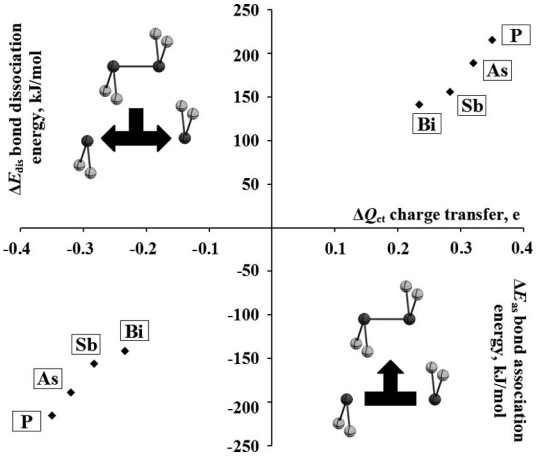

Figure 9. Calculated E–E bond association energies for $(H_3Si)_2E^{\cdot}$ and E–E bond dissociation energies for $[(H_3Si)_2E]_2$ (E = P, As, Sb, Bi) and corresponding total charge transfers on the pnicogen atoms.

provide evidence for results described above (Table 1). As a result, the $[(H_3Si)_2Bi]_2$ dimers possess the lowest stability among these compounds of pnicogens. An increase in stability of the bismuth species might be achieved by the steric bulk of the silyl substituents. For example, dibismuthanes R_4Bi_2 with little and moderate steric protection [R = Me, Et, $SiMe_3$, $CH(SiMe_3)_2$] are thermolabile and have a tendency toward disproportionation into elemental bismuth and tertiary bismuthanes $(R_3A)_3Bi$. In contrast to this, bismuthane molecules R_yBi_x (x, y = 2–4) with bulky groups [R = Ph, Mes, Si*t*Bu, $Si(SiMe_3)_3$; in our case R = *t*BuPh$_2$] are stabilized with respect to thermal decomposition.[1,3,4,31]

N-merization of n(H$_3$A)$_2$Bi$^{\cdot}$ Radicals and Oligomerization of Dimers

The *n*-merization of $(H_3A)_2Bi^{\cdot}$ radicals into $[(H_3A)_2Bi]_n$ (A = C, Si; n = 2–3) and the oligomerization associated with the formation of the systems $n[(H_3A)_2Bi]_2$ (A = C, Si; n = 2) via intermolecular Bi···Bi contacts here were evaluated by means of structure, charge, and energy calculations (Table 2, Figure 10). According to DFT computations the intramolecular Bi–Bi bond lengths in $n[(H_3A)_2Bi]_2$ elongate upon oligomerization. In $[(H_3A)_2Bi]_3$ a 3c3e bond is to be formulated. The tetramers $n[(H_3A)_2Bi]_2$ (n = 2) are a model for the oligomerization observed for R_4Bi_2 compounds in the liquid and crystalline phase. Here, rectangle and chain oligomerization has to be distinguished. Thus, the Bi_2 unit is retained and only weak intermolecular Bi···Bi contacts appear. The intermolecular Bi···Bi distances in $n[(H_3A)_2Bi]_2$ are shorter than the sum of van der Waals radii of Bi in the chain oligomerization and longer in case of the distorted rectangle oligomerization. As can be seen, the NPA bismuth charges in the silyl-substituted molecules are much lower than those in the alkyl-substituted molecules. This corresponds to better donor properties of the silyl substituents and leads to a shrinking of the covalent radius of bismuth in the alkyl derivatives. The different electronegativity of C and Si atoms, better polarization of the Bi–C bonds, which are highly polarized toward carbon atoms (ca. 70%) here, as well as two highly positive charges on neighboring Bi atoms should lead to an elongation of the intermolecular $Bi^{+Q}\cdots{}^{+Q}Bi$ bond. As a result, the repulsive van der Waals force between two alkyl-substituted dimers (A = C) dominates (Table 2). All in all, this is well expressed for the chain oligomerization. However, the distorted rectangle oligomerization reveals an inverse situation: here, the intermolecular Bi···Bi distances between alkyl-substituted dimers are slightly shorter than those between the silyl-substituted dimers. This phenomenon will be discussed later.

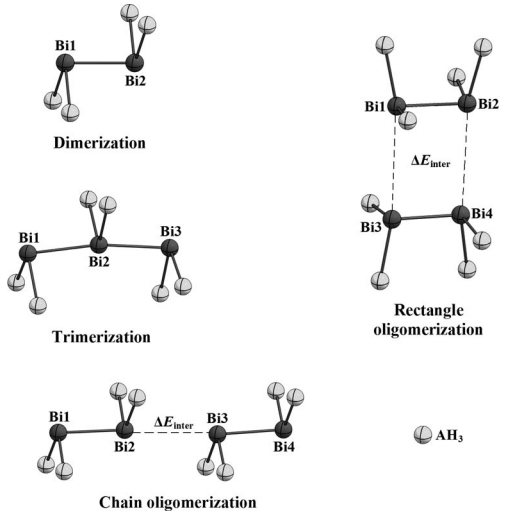

Figure 10. General view of DFT-optimized structures of $[(H_3A)_2Bi]_n$ (A = C, Si) molecules (hydrogen atoms are omitted for clarity).

The increase in the energy gain (E_n) per radical $(H_3A)_2Bi^{\cdot}$ unit for $[(H_3A)_2Bi]_n$ and $n[(H_3A)_2Bi]$ (A = C, Si) molecules listed in Table 2 indicates increased stabilization of the corresponding systems. Therefore, the silyl-substituted molecules spend more energy *per* radical unit than alkyl-substituted ones gain. The energies of the intermolecular Bi···Bi contacts (ΔE_{inter}) in the tetramers $n[(H_3A)_2Bi]_2$ (n = 2) show that for A = C the distorted rectangle oligomerization is more preferred (about 1.4 times more in the exother-

Table 2. Intermolecular properties. Computed structural parameters and calculated charges and energies for molecules $[(H_3A)_2E]_2$ (E = P, As, Sb, Bi; A = C, Si).

Parameter	$[(H_3A)_2Bi]_n$				$n[(H_3A)_2Bi]_2$			
	n = 2		n = 3		n = 2 (rectangle)		n = 2 (chain)	
	A = C	A = Si	A = C	A = Si	A = C	A = Si	A = C	A = Si
Bi1–Bi2[a]	299.9	301.4	319.4	320.2	301.4	302.5	300.8	302.6
Bi2–Bi3	–	–	319.3	319.5	–	–	392.2	379.9
Bi3–Bi4	–	–	–	–	301.4	302.5	300.7	302.5
Bi1–Bi3	–	–	–	–	424.2	429.5	–	–
Bi2–Bi4	–	–	–	–	425.3	431.5	–	–
Q_{NPA}[b]	+0.814	+0.074	+0.849 +0.773[d]	+0.127 –0.019[d]	+0.799^{av} +0.799^{av}	+0.044^{av} +0.041^{av}	+0.828 +0.793[e]	+0.099 +0.028[e]
ΔE_{mer}[c]	–130.5	–141.3	–130.4	–153.2	–277.2	–301.7	–272.4	–303.1
ΔE_{inter}[c]	–	–	–	–	–16.2	–19.1	–11.5	–20.6
E_n[c]	–65.2	–70.6	–43.5	–51.1	–69.3	–75.4	–68.1	–75.8

[a] Bi–Bi bond lengths and intermolecular Bi···Bi contacts [pm] were computed at the PBE0/BS-I level of theory. [b] The NPA charges *e* at Bi were computed at the MP2(full)/BS-II//PBE0/BS-I level. [c] Energies of *n*-merization of $(H_3A)_2Bi^{\cdot}$ radicals and energies of intermolecular contacts (ΔE_{mer} and ΔE_{inter}, respectively) [kJ/mol], as well as energy gains per radical unit (E_n) were calculated at the MP4(SDQ)/BS-II//PBE0/BS-I level. [d] NPA charge on the central Bi atom in the trimer. [e] NPA charges on intermolecular interaction centers of bismuth.

mic energy) over chain formation, whilst for A = Si the chain oligomerization is slightly more preferred. As one of the reasons, this inversion barrier at bismuth may be related to better delocalization of two high charges on Bi for A = C via the distorted rectangle, even though the Bi···Bi distances in the rectangle formation are longer than the sum of van der Waals radii of Bi. Such an effect is more weakly expressed for A = Si. An appreciable increase in the exothermic energies ΔE_{inter} with the increase in the number of $n[(H_3A)_2Bi]_2$ molecules *per* chain (n = 3) was not observed. In our opinion, the exchange of H atoms for Me groups in anti-periplanar $[(H_3Si)_2Bi]_2$ should lead to a stronger shift to chain formation on the basis of an increase in the steric strain in the molecule. Thus, the forms of the oligomerization, described above for the gas phase, could be experimentally observed for $(R_2Bi)_2$ [R = Me, $SiMe_3$; R_2 = (CMe = $CH)_2$; chain][1,32] and $\{[(Me_3Si)_2CH]_2Bi\}_2$[21] (rectangle). Here, it is necessary to remark that rectangle formation for the $\{[(Me_3Si)_2CH]_2Bi\}_2$ molecule was established in the liquid phase by NMR spectroscopy as a dynamic process of an exchange of the $[(Me_3Si)_2CH]_2Bi$ units between associated molecules, whereas in the crystalline phase, only chain formation for alkyl- and silyl-substituted dibismuthanes is well-known.[1,32] While the results obtained in the gas phase for the silyl-substituted dibismuthane molecules are in line with their experimental behavior in the crystalline phase {see $[(Me_3Si)_2Bi]_2$[1]}, the alkyl-substituted derivatives reveal various behavior. In addition, in the gas phase the intramolecular Bi–Bi bond length and the intermolecular Bi···Bi distance in the chained molecule $n[(H_3A)_2Bi]_2$ (A = C; n = 2) are 300.8 and 392.2 pm, respectively, whereas in the crystalline phase experimentally observed Bi–Bi bond length and Bi···Bi distance are 312 and 358 pm, respectively. Interestingly, the lengthening of the intramolecular Bi···Bi distance in the chained $R_4Bi_2{\cdots}Bi_2R_4$ (R = H) system to a value of 312 pm (in accordance with experimentally observed Bi–Bi bond lengths for R = Me in the crystalline phase) leads to a shortening in the intermolecular Bi···Bi distance, and as consequence, to an increase of about 11% in energy of intermolecular contacts.[33] All in all, such a difference in structure and energy behavior in the gas, liquid, and crystalline phases may be related to the temperature factor, phase transitions, as well as to an influence of the solvent molecules. All of these possible reasons demand additional investigations on such factor-dependent systems. In addition, the chain and rectangle oligomerization should strongly depend on steric strain and rigidity of the ligands. In this manner, an increase in steric strain and rigidity of the substituents on the metal atoms should lead to a moderate shift into chain formation or no oligomerization. As a result, the types of oligomerization represented above are not expected for the molecules with effectively protecting silyl (like tBuPh$_2$Si) or alkyl ligands (see Figure 3, too).

NBO Analysis

The charges (Q_{NPA}) on the bismuth atoms (natural electron configuration $6s^{1.78}6p^{3.13}$) in $[(H_3Si)_2Bi]_2$, obtained by natural population analysis (NPA) at the MP2(full) level, are slightly positive (+0.074 e). The NPA bismuth charge in $(H_3Si)_2BiBr$ is much more positive than in $[(H_3Si)_2Bi]_2$, Q_{NPA} = +0.521 e. The results of the NBO evaluations for $[(H_3Si)_2Bi]_2$ show that the bonding between bismuth centers (Bi–Bi; WBI = 0.97) is mainly carried out by p–p orbital overlap ($s^{5.0\%}p^{94.5\%}d^{0.5\%}$), (Figure 11). This overlap corresponds to the HOMO, which indicates a σ bond between the bismuth atoms (50%) (Figure 12). As a result, the $[(H_3Si)_2Bi]_2$ molecule is apolar with a dipole moment of 0 Debye. The hybrid HOMO–1, HOMO–2, HOMO–3, and HOMO–4 contain the main contributions from the Bi–Si interactions, whereas the HOMO–5 and HOMO–6 are metal lone pairs of mainly s character ($s^{78.5\%}p^{21.5\%}$; NLMO analysis provides the same result). In the polar molecule $(H_3Si)_2BiBr$ (dipole moment ca. 4 Debye), the lone pair NHO at Bi is of type s ($s^{80.1\%}p^{19.9\%}$), too.

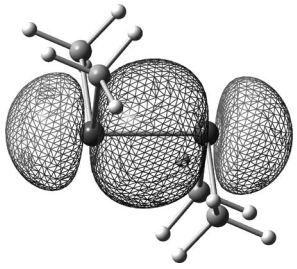

Figure 11. Graphical representation of the NBO hybrid HOMO of the model $(H_3Si)_2Bi–Bi(SiH_3)_2$.

Results from MO Theory

Figure 12 presents the frontier molecular orbitals of $[(H_3Si)_2Bi]_2$ obtained by means of canonical MO theory, which were computed at the MP4(SDQ)/BS-II//PBE0/BS-I level. Thus, according to the atomic orbital population of

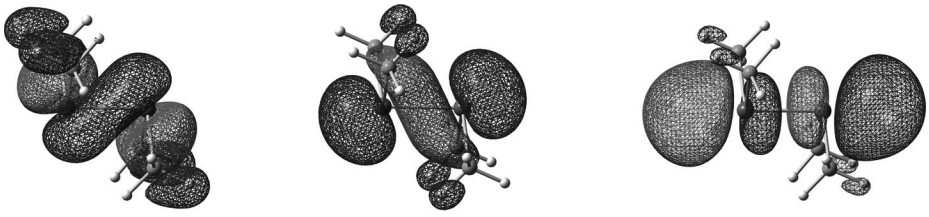

HOMO-1 **HOMO** **LUMO**

Figure 12. Graphical representation of the frontier canonical molecular orbitals of $(H_3Si)_2Bi–Bi(SiH_3)_2$ (± 0.02 isosurface value).

MOs, the components of HOMO–1 and LUMO come mainly from p orbitals of bismuth, while the HOMO contains the large s lone pair orbital parts of bismuth.

According to results of MO theory, the s LPs on Bi in model compound $[(H_3Si)_2Bi]_2$ with non-overloaded silyl substituents correspond to the HOMO. Interactions through these LPs are known and were observed in the reactions of tBu$_3$M with Bi_2Et_4, resulting in Lewis acid–base adducts $[Et_4Bi_2][Mt Bu_3]_2$ (where M = Al, Ga).[34] An increase in steric protection of the substituents should lead to a decrease in activity of the s LPs, and accordingly to an increase in stereochemical inert character. Therefore, the stereochemically active role of the LPs of bismuth in **2** is expressed very weakly. The s LP of **3** corresponds to the HOMO, too.

Interestingly, the HOMO–LUMO ΔE gap for $[(H_3Si)_2Bi]_n$ decreases upon oligomerization (Figure 13). Thus, delocalization of p electrons of $(H_3Si)_2Bi^{\cdot}$ radicals (ΔE = 9.43 eV) in the Bi–Bi bond (the Bi–Bi stretching frequency is 127 cm^{-1}) leads to the reduction of ΔE toward 8.73 eV (n = 2). The Bi–Bi chain-oligomerized forms, $n[(H_3Si)_2Bi]_2$, have gaps of 7.75 eV (n = 2) and 7.24 eV (n = 3), accordingly. The values of the first ionization potentials (IP = E_{HOMO}; on the basis of the Koopman's theorem) and the energy values of the lowest occupied molecular orbitals decrease, accordingly. According to DFT-optimized geometries of the $n[(H_3Si)_2Bi]_2$ systems (n = 1–3), the interaction between intermolecular Bi centers in the chain provides a moderate elongation of the intramolecular Bi–Bi bond in the dibismuthane unit from 301.4 pm for n = 1 through 302.5/302.6 pm for n = 2 toward 302.6/302.7 and 303.9 pm (central unit) for n = 3. In addition, this leads to a shorting of the intermolecular Bi···Bi contacts from 379.9 pm for n = 2 toward 378.2 pm (average) for n = 3.

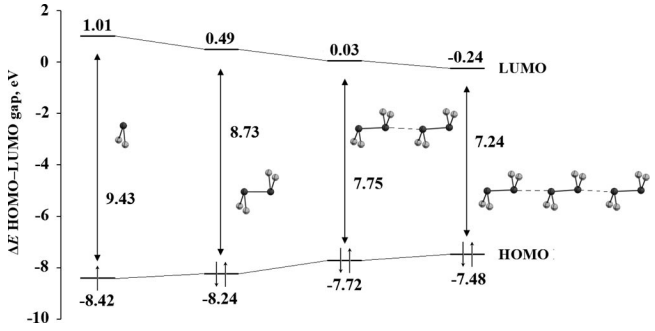

Figure 13. Changes in the HOMO–LUMO energy gap for $n(H_3Si)_2Bi^{\cdot}$ (n = 1–2) and $n[(H_3Si)_2Bi]_2$ (n = 2–3) systems upon n-merization and chain oligomerization, respectively.

As can be seen in Figure 14, the intermolecular interactions in the chained $[(H_3Si)_2Bi]_2\cdots[Bi(SiH_3)_2]_2$ molecule correspond to the bonding HOMO-1 (s LP orbitals that are bound together) and HOMO-3 (p-type orbitals that are bound together) and the LUMO with overlapping intermolecular p* orbitals, whereas the HOMO and the HOMO-2 are intermolecular antibonding in nature and correspond to the intramolecular interactions in each dimer molecule $[(H_3Si)_2Bi]_2$ (as described in Figure 12). As a result of the $[(H_3Si)_2Bi]_2\cdots[Bi(SiH_3)_2]_2$ intermolecular interaction, the charges on the bismuth interacting centers are reduced from +0.074 e in dimer $[(H_3Si)_2Bi]_2$ to + 0.028 e in oligomer $[(H_3Si)_2Bi]_2\cdots[Bi(SiH_3)_2]_2$, whereas the charges on the non-interacting bismuth centers become slightly more positive + 0.099 e, accordingly. This induced dipole causes an electrostatic attraction between these two nonpolar molecules. Thus, the dipole moment of $[(H_3Si)_2Bi]_2$ is 0 Debye, whereas that of $[(H_3Si)_2Bi]_2\cdots[Bi(SiH_3)_2]_2$ becomes more positive, 0.46 Debye. In addition, such Bi···Bi intermolecular attraction is very weak (0.04) according to the WBI. This fact and the small charges involved here, as well as the absence of other intermolecular contacts, point to the London dispersion force.

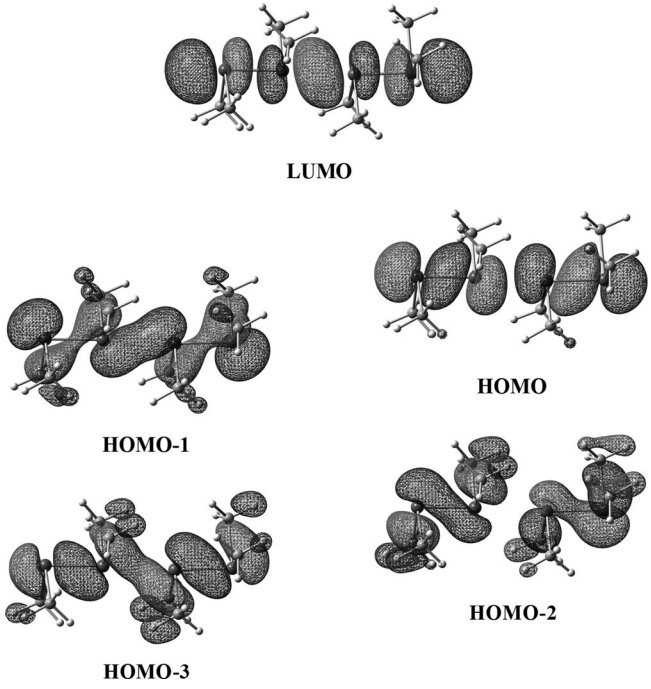

Figure 14. Graphical representation of the frontier canonical molecular orbitals of $[(H_3Si)_2Bi]_2\cdots[Bi(SiH_3)_2]_2$ upon oligomerization (± 0.02 isosurface value).

TD-DFT Computations

According to time-dependent (TD) DFT computations of vertical electronic transitions in $[(H_3Si)_2Bi]_2$, the lowest energy $S_0 \rightarrow S_1$ electronic transition corresponds to the HOMO → LUMO and HOMO–1 → LUMO excitations with a predominantly $n_{Bi(s,p)} \rightarrow n^*_{Bi(p)}$ character. The transitions are in the near UV region (301 nm, 4.12 eV, 33 223 cm^{-1}). Such electron transfer can be described as metal–metal charge transfer (MMCT excitation). Intermolecular interaction of s LPs of the Bi–Bi bond in the bismuth chain-oligomerized form (Figures 13, 14) leads to a bathochromic shift toward lower frequencies. Thus, the lowest energy electronic transitions for $n[(H_3Si)_2Bi]_2$ are 301 (n = 1), 347 (n = 2), and 391 nm (n = 3). This fits well with the results described above (Figure 13). Experimentally, a change in color is observed for $[(Me_3Si)_2Bi]_2$[1] upon transition between the fluid phase {red $[(Me_3Si)_2Bi]_2$} and the crystalline phase

{green $n[(Me_3Si)_2Bi]_2$, where n is the number of molecules in the Bi chain}. These results are in contrast to those obtained for **2**, which is "nonthermochromic" dibismuthane. In addition, a maximum absorption band for the compounds with more bulky silyl ligands should be shifted to lower energy, too. The absorption spectrum of **2** in toluene provides evidence for this. Thus, the observed lowest energy absorption maximum lies at 465 nm (2.67 eV, 21 505 cm^{-1}) in the visible spectral region and is close to the value of the $S_0 \rightarrow S_1$ electronic transition (the HOMO → LUMO and HOMO–2 → LUMO excitations) determined computationally by using the fixed structure of **2** from X-ray crystallography (418 nm, 2.97 eV, 23 923 cm^{-1}).

Conclusions

By the reactions of $BiBr_3$ with various amounts of the bulky lithium silanide **1**, the formation of Bi–Bi bonded product **2** could be observed. However, **2** was isolated only from the redox reaction in 1:3 ratio, as a main product. The formation of tertiary bismuthane $(t\text{BuPh}_2\text{Si})_3\text{Bi}$ was not observed. This is probably due to steric reasons. Accordingly, no oligomerization of **2** is observed. This is in contrast to the observation that $Bi_2(SiMe_3)_4$ is "thermochromic",[1] where oligomerization via Bi···Bi contacts is observed. In all reactions, both metathesis and redox processes were observed. These led to the formation of Bi–Br bonded product **3** simultaneously with **2**.

The bulky $SiPh_2t\text{Bu}$ ligand is a valuable source, which should promote the radicalization processes in the reactions of trigonal pyramidal structural units (like EX_3) of the group 15 elements (E = P, As, Sb, Bi) with alkali metal silanide $M(sol)_nSiPh_2t\text{Bu}$ (M = Li, Na, K; n = 0–3) on the basis of the shape of the silyl substituents (steric factor) and "hybridization sp valence orbital effect" of the corresponding element E (electronic factor).

Dibismuthanes such as **2** are potentially useful and important starting reagents for further synthetic applications. On one hand, these may react via the s LPs of Bi as σ-donor, to form Lewis acid–base adducts;[34] on the other hand, the more sterically demanding alkyl or silyl groups (like those in **2**) are, the less stereochemically active these orbitals are. This is due to the increasing protection of the metal center in the molecules. Finally, such compounds with Bi–Bi bonds open a way to ring systems or to bismuth species in its +1 oxidation state, for example.[31b] Sterically protecting ligands should play a key role and determine all probabilities of reaction of the complexes.

Experimental Section

General: All manipulations were carried out with the use of standard Schlenk techniques under an oxygen-free and water-free argon atmosphere and in vacuo. All organic solvents were distilled, dried, and degassed according to standard procedures. Hexane and toluene were dried with sodium/benzophenone and freshly distilled under argon. $Li(thf)_3SiPh_2t\text{Bu}$ (**1**), was prepared according to a literature procedure.[13] Elemental analysis was performed in the microanalytical laboratory of Ruprecht-Karls-University of Heidelberg. ^1H, ^{13}C, and ^{29}Si NMR spectra were recorded with a Bruker Advance-400 (399.89, 100.55, and 79.44 MHz for ^1H, ^{13}C, and ^{29}Si analyses, respectively) instrument. Chemical shifts are reported in δ units (ppm) and are referenced to an external standard of tetramethylsilane (TMS) $SiMe_4$ (δ = 0.00 ppm) and benzene C_6D_6 (δ = 7.13 ppm). Electronic spectra were measured at room temp. under an argon atmosphere with a Tidas II J&M spectrophotometer, using toluene as solvent. The LIFDI-MS was recorded with a JEOL JMS-700 operating in the positive ion mode with full scanning in the range 200–1800; compound **2** was supplied as dilute solutions at about 0.2 mg mL^{-1} in toluene.

Crystal Structure Determination: X-ray data for single crystals of **1**–**3** were collected with a STOE IPDS I diffractometer equipped with an image plate area detector, using a graphite monochromator (Mo-K_α) (λ = 71.073 pm). The structure was refined against all F^2 data by full-matrix least-squares techniques (SHELXT 5.01; PC Version, Siemens, Bruker AXS).[35] All non-hydrogen atoms were refined with anisotropic thermal parameters. All H atoms were placed in calculated positions and refined by using a riding model. A summary of crystal data and structure refinements for the compounds are listed in Table 3. CCDC-742475 (**1**), -742476 (**2**·$2C_6H_5Me$), -742477 (**3**), and -742909 ($t\text{BuPh}_2\text{Si}$) contain the supplementary crystallographic data for this paper. These data can be obtained free of charge from The Cambridge Crystallographic Data Centre via www.ccdc.cam.ac.uk/data_request/cif.

Compound 2: A suspension of (2.93 g, 6.34 mmol) $Li(thf)_3Sit\text{BuPh}_2$ (**1**) in toluene (20 mL) was added dropwise to a stirred solution of (0.95 g, 2.11 mmol) $BiBr_3$ in toluene (40 mL) at –78 °C. The dark-colored reaction mixture was stirred for an additional 3 h at low temperature and was then slowly warmed to ambient temperature. Initially, a green solution was observed. After stirring for 16 h, all volatile reaction components were removed with an oil vacuum pump. The residue was extracted with hexane (60 mL) and then with toluene (60 mL). After filtration, dark-red solutions were obtained. The hexane and toluene fractions show similar ^{29}Si NMR signals. The toluene and solutions were reduced to a volume of 15 mL and cooled to –20 °C, resulting in the formation of dark-red crystals of **2**; yield: 1.88 g (64%; with reference to Bi). Compound **2** is soluble in organic solvents and stable in the range –30–100 °C. $C_{64}H_{76}Bi_2Si_4$ (1374.46): calcd. C 55.88, H 5.57; found C 55.69, H 6.05. ^1H NMR (400 MHz, C_6D_6, iTMS): δ = 1.12 (s, CMe_3, 1), 7.58 (m, *o*-Ph), 7.67 (m, *p*-Ph), 7.79 (m, *m*-Ph) ppm. ^{13}C NMR (100.55 MHz, C_6D_6, iTMS): δ = 26.8 (s, *C*Me_3), 30.4 (s, CMe_3), 129.7 (*m*-Ph), 132.6 (*p*-Ph), 136.0 (*o*-Ph), 138.2 (*i*-Ph) ppm. ^{29}Si NMR (79.44 MHz, C_6D_6, eTMS): δ = 15.9 (s, *Si*$Ph_2t\text{Bu}$) ppm. UV/Vis (toluene): λ_{max} (ε, L mol^{-1} cm^{-1}) = 465 (2132) nm. LIFDI-MS (toluene): m/z (%) = 1374.6 (100) $[M]^+$, 1135.4 (13) $[M^+ - SiPh_2t\text{Bu}]$, 687.3 (18) $[(t\text{BuPh}_2\text{Si})_2\text{Bi}]^+$, 447.3 (5) $[(t\text{BuPh}_2\text{Si})\text{Bi}]^+$.

Compound 3: A suspension of (3.06 g, 6.63 mmol) (**1**) in toluene (20 mL) was added dropwise to a stirred solution of (1.49 g 3.31 mmol) $BiBr_3$ in toluene (40 mL) at –78 °C. The dark-colored reaction mixture was stirred for an additional 3 h at low temperature and was then slowly warmed to ambient temperature. After stirring for 16 h, all volatile reaction components were removed with an oil vacuum pump, and the residue was extracted first with hexane (60 mL) and then with toluene (60 mL). After filtration of the hexane and toluene fractions, the dark-green (denoted "DGS") and red (denoted "RS") solutions were obtained, respectively. Hexane and toluene solutions were reduced to a volume 15 mL and

Table 3. Crystal data and structure refinement details for **1**–**3**.

	1	**2**·2C_6H_5Me	**3**
Empirical formula	$C_{28}H_{43}LiO_3Si$	$C_{78}H_{92}Bi_2Si_4$	$C_{32}H_{38}BiBrSi_2$
Formula weight [g/mol]	462.32	1559.84	767.69
Temperature [K]	200	200	200
Crystal color	pale green	dark red	red
Crystal size [mm]^3	$0.37 \times 0.35 \times 0.24$	$0.3 \times 0.16 \times 0.07$	$0.41 \times 0.14 \times 0.06$
Crystal system	monoclinic	triclinic	orthorhombic
Space group	$P2_1/n$	$P\bar{1}$	$P2_1\ 2_1\ 2_1$
a [pm]	1018.6(2)	1368.8(3)	1044.1(2)
b [pm]	1711.3(3)	1421.5(3)	1150.9(2)
c [pm]	4808(1)	1848.0(4)	2526.2(5)
α [°]		96.01(3)	
β [°]	90.08(3)	92.84(3)	
γ [°]		101.42(3)	
V [Å^3]	8381(3)	3496(1)	3035(1)
Z	12	2	4
D_{calc} [Mg/m^3]	1.099	1.482	1.680
μ (Mo-K_α) [mm^{-1}]	0.109	5.137	7.223
F(000)	3020	1564	1504
2θ-range [°]	2.04–26.13	2.52–30.63	2.11–28.15
Abs. corr.	numerical	numerical	numerical
Min/max transm.	0.9618/0.9832	0.255/0.674	0.1945/0.5230
Index ranges	$-12 \le h \le 12$	$-19 \le h \le 19$	$-13 \le h \le 13$
	$-21 \le k \le 21$	$-20 \le k \le 19$	$-15 \le k \le 14$
	$-59 \le l \le 59$	$-26 \le l \le 26$	$-33 \le l \le 33$
Reflections collected	36694	42336	29770
Independent reflections	14556	19419	7354
Observed refl. [$I > 2\sigma(I)$]	6160	9297	6592
Data/restraints/parameters	14556/0/912	19419/0/757	7354/0/326
Goodness-of-fit (S) on F^2	0.842	0.774	0.923
Final R indices [$I > 2\sigma(I)$]	$R1$ = 0.0630	$R1$ = 0.0515,	$R1$ = 0.0248,
	wR_2 = 0.1291	wR_2 = 0.1055	wR_2 = 0.0509
R indices (all data)	$R1$ = 0.1463	$R1$ = 0.1249,	$R1$ = 0.0307,
	wR_2 = 0.1553	wR_2 = 0.1235	wR_2 = 0.0521
Largest diff. peak/hole [e nm^{-3}]	214/–192	2578/–3067	1121/–548

cooled to –20 °C, resulting in the formation of only red crystals of **3**. ^{29}Si NMR spectra for both solutions contain the silicon signals of **2** and disilane, too. Yield of DGS: 0.91 g (35.7%; with reference to Bi). Yield of RS: 0.48 g (19.0%; with reference to Bi). After short periods of time at –20 °C or at room temp., both solutions decompose with formation of elemental bismuth. The crystals of **2** (which form predominantly) also were obtained by this reaction in a 1:1 ratio (^{29}Si NMR signals of **2** and disilane were observed, too).

DGS: The signals of **2** and disilane are omitted. ^{1}H NMR (400 MHz, C_6D_6, iTMS): δ = 7.87 (m, *m*-Ph), 7.71 (m, *p*-Ph), 7.49 (m, *o*-Ph), 1.21 (s, C*Me*$_3$) ppm. ^{13}C NMR (100.55 MHz, C_6D_6, iTMS): δ = 138.5 (*i*-Ph), 137.1 (*o*-Ph), 133.3 (*p*-Ph), 130.0 (*m*-Ph), 31.2 (s, C*Me*$_3$), 27.0 (s, *C*Me$_3$) ppm. ^{29}Si NMR (79.44 MHz, C_6D_6, eTMS): δ = –4.2 (s, *Si*Ph$_2$*t*Bu) ppm.

RS: The signals of **2**, disilane, and DGS are omitted. ^{1}H NMR (400 MHz, C_6D_6, iTMS): δ = 7.74 (m, *m*-Ph), 7.63 (m, *p*-Ph), 7.29 (m, *o*-Ph), 1.14 (s, C*Me*$_3$) ppm. ^{13}C NMR (100.55 MHz, C_6D_6, iTMS): δ = 138.3 (*i*-Ph), 136.3 (*o*-Ph), 132.7 (*p*-Ph), 129.9 (*m*-Ph), 31.1 (s, C*Me*$_3$), 27.6 (s, *C*Me$_3$) ppm. ^{29}Si NMR (79.44 MHz, C_6D_6, eTMS): δ = –6.1 (s, *Si*Ph$_2$*t*Bu) ppm.

Computational Methods: DFT structure optimizations were performed with the Turbomole program,[36] adopting the multiple "M3" grid size for the density fitting and a SCF convergence criterion of 1×10^{-7} E_h. The initial geometries were fully optimized with the hybrid exchange-correlation functional PBE0.[37] As Gaussian AO basis for all atoms, all-electron split valence SV(P) sets of def2-type[38] were employed (Basis Set System I, which is denoted BS-I). All other computations were carried out on PBE0 optimized geometries with the Gaussian 03 program package.[39] We used Los Alamos National Laboratory 2 (LANL2) relativistic effective core potentials (RECPs) to describe the core electrons of In, P, As, Sb, Bi, and Br atoms and employed split-valence (double-ζ) quality basis sets to describe their s and p valence electrons. For P, As, Sb, Bi, and Br atoms, the LANL2DZ basis set was augmented by adding one set of polarization and one set of diffuse functions.[40] For Si, C, and H atoms, all-electron split-valence 6-311+G(d,p) basis sets supplemented with a single set of diffuse functions on carbon and silicon atoms were employed.[41] The combination of LANL2DZdp and 6-311+G(d,p) is denoted Basis Set System II (BS-II). The vibrational frequencies were evaluated on all DFT-optimized geometries by using the HF method to verify their status as true local minima on the potential energy surface and to obtain zero-point corrections to the energies (ZPE) without scaling. The nature of the chemical bonding was analyzed by means of the NBO approach with the second-order Møller–Plesset perturbation theory, including all valence electrons in the configuration space [MP2(full)]. The atomic charges were computed within the natural population analysis (NPA). Wiberg indexes were evaluated and used as bond strength indicators. NBO analyses were performed with NBO Version 3.1[42] incorporated in the Gaussian 03 program. To gain insight into the vertical singlet electronic states, time-dependent functional theory[43] (TD-PBE0 method) calculations were performed. Energies reported herein were evaluated by using the fourth-order Møller–Plesset perturbation theory [MP4(SDQ)] in combination with PBE0 parameterization.

Acknowledgments

We are grateful to the Graduate College 850 "Molecular Modeling" of the German Research Foundation (DFG) for financial support. We also thank Philipp Butzug for assistance in collecting the crystallographic data sets.

[1] a) O. Mundt, G. Becker, M. Rössler, C. Witthauer, *Z. Anorg. Allg. Chem.* **1983**, *506*, 42–58; b) G. Becker, O. Mundt in *Unkonventionelle Wechselwirkungen in der Chemie metallischer Elemente*, VCH, Weinheim, **1992**, pp. 199–217.
[2] G. M. Kollegger, H. Siegl, K. Hassler, K. Gruber, *Organometallics* **1996**, *15*, 4337–4338.
[3] a) G. Linti, W. Köstler, *Z. Anorg. Allg. Chem.* **2002**, *628*, 63–66; b) G. Linti, W. Köstler, H. Pritzkow, *Eur. J. Inorg. Chem.* **2002**, 2643–2647.
[4] C. von Hänisch, D. Nikolova, *Eur. J. Inorg. Chem.* **2006**, 4770–4773.
[5] S. Schulz, M. Nieger, *Angew. Chem.* **1999**, *111*, 1020–1021; *Angew. Chem. Int. Ed.* **1999**, *38*, 967–968.
[6] A. Kuczkowski, F. Thomas, S. Schulz, M. Nieger, *Organometallics* **2000**, *19*, 5758–5762.
[7] A. Kuczkowski, S. Schulz, M. Nieger, *Eur. J. Inorg. Chem.* **2001**, 2605–2611.
[8] A. Kuczkowski, S. Schulz, M. Nieger, P. R. Schreiner, *Organometallics* **2002**, *21*, 1408–1419.
[9] F. Thomas, S. Schulz, M. Nieger, *Organometallics* **2002**, *21*, 2793–2795.
[10] D. Fenske, A. Rothenberger, S. Wieber, *Z. Anorg. Allg. Chem.* **2003**, *629*, 929–930.
[11] F. Thomas, S. Schulz, H. Mansikkamäki, M. Nieger, *Angew. Chem.* **2003**, *115*, 5800–5803; *Angew. Chem. Int. Ed.* **2003**, *42*, 5641–5644.
[12] R. Wolf, J. Fischer, R. C. Fischer, J. C. Fettinger, P. P. Power, *Eur. J. Inorg. Chem.* **2008**, 2515–2521.
[13] B. K. Campion, R. H. Heyn, T. D. Tilley, *Organometallics* **1993**, *12*, 2584–2590.
[14] K. H. Ebert, R. E. Schulz, H. J. Breunig, C. Silvestru, I. Haiduc, *J. Organomet. Chem.* **1994**, *470*, 93–98.
[15] C. Strohmann, O. Ulbrich, D. Auer, *Eur. J. Inorg. Chem.* **2001**, 1013–1018.
[16] a) H. V. R. Dias, M. M. Olmstead, K. Ruhlandt-Senge, P. P. Power, *J. Organomet. Chem.* **1993**, *462*, 1–6; b) A. Heine, R. Herbst-Irmer, G. M. Sheldrick, D. Stalke, *Inorg. Chem.* **1993**, *32*, 2694–2698.
[17] N. Wiberg, K. Ameluxen, H.-W. Lerner, H. Schuster, H. Nöth, I. Krossing, M. Schmidt-Ameluxen, T. Seifert, *J. Organomet. Chem.* **1997**, *542*, 1–18.
[18] H.-W. Lerner, I. Sänger, F. Schödel, K. Polborn, M. Bolte, M. Wagner, *Z. Naturforsch., Teil B* **2007**, *62*, 1285–1290.
[19] A. Kawachi, K. Tamao, *J. Am. Chem. Soc.* **2000**, *122*, 1919–1926.
[20] Y. Apeloig, M. Yuzefovich, M. Bendikov, D. Bravo-Zhivotovskii, D. Bläser, R. Boese, *Angew. Chem. Int. Ed.* **2001**, *40*, 3016–3020.
[21] G. Balázs, H. J. Breunig, E. Lork, *Organometallics* **2002**, *21*, 2584–2586.
[22] C. Silvestru, H. J. Breunig, H. Althaus, *Chem. Rev.* **1999**, *99*, 3277–3327.
[23] H. Althaus, H. J. Breunig, R. Rösler, E. Lork, *Organometallics* **1999**, *18*, 328–331.
[24] B. Murray, J. Hvoslef, H. Hope, P. P. Power, *Inorg. Chem.* **1983**, *22*, 3421.
[25] G. Linti, M. Bühler, K. Yu. Monakhov, T. Zessin, *Dalton Trans.* **2009**, 8071–9078.
[26] a) S. L. Hinchley, C. A. Morrison, D. W. H. Rankin, C. L. B. Macdonald, R. J. Wiacek, A. H. Cowley, M. F. Lappert, G. Gundersen, J. A. C. Clyburne, P. P. Power, *Chem. Commun.* **2000**, 2045; b) S. L. Hinchley, C. A. Morrison, D. W. H. Rankin, C. L. B. Macdonald, R. J. Wiacek, A. Voigt, A. H. Cowley, M. F. Lappert, G. Gundersen, J. A. C. Clyburne, P. P. Power, *J. Am. Chem. Soc.* **2001**, *123*, 9045–9053.
[27] a) M. J. S. Gynane, A. Hudson, M. F. Lappert, P. P. Power, H. Goldwhite, *J. Chem. Soc., Dalton Trans.* **1980**, 2428–2433; b) P. P. Power, *Chem. Rev.* **2003**, *103*, 789–809.
[28] N. S. Vyazankin, G. A. Razuvaev, O. A. Kruglaya, G. S. Semchikova, *J. Organomet. Chem.* **1966**, *6*, 474.
[29] L. Balázs, H. J. Breunig, E. Lork, A. Soran, C. Silvestru, *Inorg. Chem.* **2006**, *45*, 2341–2346.
[30] a) H. Gilman, H. L. Yablunky, *J. Am. Chem. Soc.* **1941**, *63*, 212–216; b) H. Gilman, H. L. Yale, *Chem. Rev.* **1942**, *30*, 281–320.
[31] a) A. J. Ashe III, E. G. Ludwig Jr., J. Oleksyszyn, *Organometallics* **1983**, *2*, 1859–1866; b) H. J. Breunig, *Z. Anorg. Allg. Chem.* **2005**, *631*, 621–631.
[32] a) O. Mundt, H. Riffel, G. Becker, A. Simon, *Z. Naturforsch., Teil B* **1988**, *43*, 952; b) A. J. Ashe III, J. W. Kampf, D. B. Puranik, S. M. Al-Taweel, *Organometallics* **1992**, *11*, 2743–2745.
[33] K. W. Klinkhammer, P. Pyykkö, *Inorg. Chem.* **1995**, *34*, 4134–4138.
[34] A. Kuczkowski, S. Schulz, M. Nieger, *Angew. Chem.* **2001**, *113*, 4351–4353; *Angew. Chem. Int. Ed.* **2001**, *40*, 4222–4225.
[35] G. M. Sheldrick, *Acta Crystallogr., Sect. A* **2008**, *64*, 112–122.
[36] R. Ahlrichs, M. Bär, M. Häser, H. Horn, C. Kölmel, *Chem. Phys. Lett.* **1989**, *162*, 165–169.
[37] C. Adamo, V. Barone, *J. Chem. Phys.* **1999**, *110*, 6158.
[38] a) B. Metz, H. Stoll, M. Dolg, *J. Chem. Phys.* **2000**, *113*, 2563–2569; b) F. Weigend, R. Ahlrichs, *Phys. Chem. Chem. Phys.* **2005**, *7*/*18*, 3297–3305.
[39] M. J. Frisch, G. W. Trucks, H. B. Schlegel, G. E. Scuseria, M. A. Robb, J. R. Cheeseman, J. A. Montgomery Jr., T. Vreven, K. N. Kudin, J. C. Burant, J. M. Millam, S. S. Iyengar, J. Tomasi, V. Barone, B. Mennucci, M. Cossi, G. Scalmani, N. Rega, G. A. Petersson, H. Nakatsuji, M. Hada, M. Ehara, K. Toyota, R. Fukuda, J. Hasegawa, M. Ishida, T. Nakajima, Y. Honda, O. Kitao, H. Nakai, M. Klene, X. Li, J. E. Knox, H. P. Hratchian, J. B. Cross, V. Bakken, C. Adamo, J. Jaramillo, R. Gomperts, R. E. Stratmann, O. Yazyev, A. J. Austin, R. Cammi, C. Pomelli, J. W. Ochterski, P. Y. Ayala, K. Morokuma, G. A. Voth, P. Salvador, J. J. Dannenberg, V. G. Zakrzewski, S. Dapprich, A. D. Daniels, M. C. Strain, O. Farkas, D. K. Malick, A. D. Rabuck, K. Raghavachari, J. B. Foresman, J. V. Ortiz, Q. Cui, A. G. Baboul, S. Clifford, J. Cioslowski, B. B. Stefanov, G. Liu, A. Liashenko, P. Piskorz, I. Komaromi, R. L. Martin, D. J. Fox, T. Keith, M. A. Al-Laham, C. Y. Peng, A. Nanayakkara, M. Challacombe, P. M. W. Gill, B. Johnson, W. Chen, M. W. Wong, C. Gonzalez, and J. A. Pople, *Gaussian 03*, Revision E. 01, Gaussian, Inc., Wallingford CT, **2004**.
[40] a) P. J. Hay, W. R. Wadt, *J. Chem. Phys.* **1985**, *82*, 270; b) P. J. Hay, W. R. Wadt, *J. Chem. Phys.* **1985**, *82*, 284; c) P. J. Hay, W. R. Wadt, *J. Chem. Phys.* **1985**, *82*, 299; d) C. E. Check, T. O. Faust, J. M. Bailey, B. J. Wright, T. M. Gilbert, L. S. Sunderlin, *J. Phys. Chem. A* **2001**, *105*, 8111.
[41] a) R. Krishnan, J. S. Binkley, R. Seeger, J. A. Pople, *J. Chem. Phys.* **1980**, *72*, 650; b) T. Clark, J. Chandrasekhar, P. v. R. Schleyer, *J. Comput. Chem.* **1983**, *4*, 294.
[42] a) E. D. Glendening, A. E. Reed, J. E. Carpenter, F. Weinhold, *NBO program*, vers. 3.1; b) A. E. Reed, L. A. Curtiss, F. Weinhold, *Chem. Rev.* **1988**, *88*, 899.
[43] M. E. Casida, C. Jaorski, K. C. Casida, D. R. Salahub, *J. Chem. Phys.* **1998**, *108*, 4439.

Received: August 6, 2009
Published Online: November 27, 2009

